Received: 4 February 2024 | Accepted: 8 July 2024

DOI: 10.1111/mice.13326

COMPUTER-AIDED CIVIL AND INFRASTRUCTURE ENGINEERING WILEY

RESEARCH ARTICLE

Prediction of stratified ground consolidation via a physics-informed neural network utilizing short-term excess pore water pressure monitoring data

Weibing Gong[1] | **Linlong Zuo**[2] | **Lin Li**[2] | **Hui Wang**[3]

[1]Department of Earth Sciences and Engineering, Missouri University of Science and Technology, Rolla, Missouri, USA

[2]School of Highway, Chang'an University, Xi'an, Shaanxi, China

[3]Department of Engineering Science, University of Oxford, Oxford, UK

Correspondence
Lin Li, School of Highway, Chang'an University, Xi'an, Shaanxi 710064, China.
Email: lilin_sanmao@163.com

Hui Wang, Department of Engineering Science, University of Oxford, Oxford, UK.
Email: hui.wang@eng.ox.ac.uk

Funding information
National Natural Science Foundation of China, Grant/Award Number: 52108297; Postdoctoral Research Foundation of China, Grant/Award Number: 2021M692742; Special Support Project of the China Postdoctoral Science Foundation, Grant/Award Number: 2023T160560; Qin Chuang Yuan Imported High-level Innovation and Entrepreneurship Talent Project, Grant/Award Number: OCYRCXM-2022-29; Fundamental Research Funds for the Central Universities, Grant/Award Number: 300102212301

Abstract

Predicting stratified ground consolidation effectively remains a challenge in geotechnical engineering, especially when it comes to quickly and dependably determining the coefficient of consolidation (c_v) for each soil layer. This difficulty primarily stems from the time-intensive nature of the consolidation process and the challenges in efficiently simulating this process in laboratory settings and using numerical methods. Nevertheless, the consolidation of stratified ground is crucial because it governs ground settlement, affecting the safety and serviceability of structures situated on or in such ground. In this study, an innovative method utilizing a physics-informed neural network (PINN) is introduced to predict stratified ground consolidation, relying solely on short-term excess pore water pressure (PWP) data collected by monitoring sensors. The proposed PINN framework identifies c_v from the limited PWP data set and subsequently utilizes the identified c_v to predict the long-term consolidation process of stratified ground. The efficacy of the method is demonstrated through its application to a case study involving two-layer ground consolidation, with comparisons made to an existing PINN method and a laboratory consolidation test. The results of the case study demonstrate the applicability of the proposed PINN method to both forward and inverse consolidation problems. Specifically, the method accurately predicts the long-term dissipation of excess PWP when c_v is known (i.e., the forward problem). It successfully identifies the unknown c_v with only 0.05-year monitoring data comprising 10 data points and predicts the dissipation of excess PWP at 1-year, 10-year, 15-year, and even up to 30-year intervals using the identified c_v (i.e., the inverse problem). Moreover, the investigation into optimal PWP monitoring sensor layouts reveals that installing sensors in areas with significant variations in excess PWP enhances the prediction accuracy of the proposed PINN method. The results underscore the potential of leveraging PINNs in

conjunction with PWP monitoring sensors to effectively predict stratified ground consolidation.

1 | INTRODUCTION

Soil consolidation is a phenomenon that occurs when soil experiences a reduction in volume due to the dissipation of water from its pores, namely, the dissipation of excess PWP, under the influence of external loads, such as those from construction activities and the weight of buildings. This process can lead to ground settlement, impacting the stability and integrity of structures erected on or within the ground, particularly in instances of uneven settlement. A key parameter in evaluating soil consolidation is c_v, which considers the soil properties that control the consolidation rate. A larger c_v signifies more rapid dissipation of excess PWP and, consequently, a quicker consolidation process. c_v is extensively utilized for estimating settlement timing (e.g., Duncan, 1993; Shukla et al., 2009), analyzing soil behavior (e.g., Cargill, 1984; Gong et al., 2017), designing geotechnical structures (e.g., Gong et al., 2020; Li et al., 2017), and addressing settlement-related issues (e.g., Horpibulsuk et al., 2012; Lu et al., 2017).

Currently, primary methods for determining c_v include laboratory-empirical approaches, in situ measurements, and numerical simulations. Among the laboratory-empirical methods, time-fitting logarithm method (i.e., Casagrande's method) and time-fitting square root method (i.e., Taylor's method) are prevalent. Despite the widespread application of laboratory-empirical methods in determining c_v, it is imperative to acknowledge that laboratory-derived values are susceptible to significant influences from various factors, including soil sample disturbance, load increment ratio, laboratory duration, and temperature (Holtz et al., 2011). Moreover, laboratory tests encounter challenges related to scaling and boundary conditions, given that small laboratory samples may not accurately represent the extensive in situ soil mass. Furthermore, the boundary conditions in laboratory tests (e.g., the rigid walls of consolidation cells) present a simplified scenario compared to the multifaceted and variable conditions encountered in the field.

To address the limitations associated with laboratory-empirical methods, in situ field tests (e.g., Alzubaidi, 2020; Clarke, 1990) have been developed to determine c_v. Prominent in situ testing methodologies include the piezocone penetration test (CPTu), pressuremeter test, and dilatometer test (DMT). While in situ testing methods for measuring c_v offer advantages, such as the assessment under natural soil conditions, minimal sample disturbance, and the capability to acquire continuous data across different soil depths, they are not without challenges. Deriving c_v from these in situ tests often requires methods such as empirical relationships or curve fitting, which are subject to human error. This human error can stem from various sources, including data collection inaccuracies, the selection of empirical relationships (which may yield different results based on the engineer experience and judgment), the subjective nature of curve fitting techniques, and potential biases in data interpretation. In addition, other challenges include the indirect nature of c_v measurement and the requirement for specialized equipment and expertise.

Numerical methods are increasingly gaining popularity for determining c_v, particularly for scenarios that pose challenges to traditional methods. The numerical approaches applied in this context include finite element methods (FEMs; e.g., Jang et al., 2003), finite difference methods (e.g., Abbasi et al., 2007), and boundary element methods (e.g., Chiou & Chi, 1994). These methods facilitate the simulation of the consolidation process under varied loading conditions, taking into account the heterogeneity, anisotropy, and nonlinear behavior of soil properties, which are the key advantages of numerical simulations. However, these methods also present several limitations compared to PINN methods, including (a) PINNs can integrate observational data directly into the modeling process, which helps in automatically learning complex patterns and relationships in the data. This capability reduces the dependency on advanced knowledge of soil mechanics and constitutive modeling. (b) PINNs exhibit a high degree of flexibility, allowing them to adapt to various problem settings without necessitating significant modifications to their underlying framework. In contrast, numerical methods, such as FEMs, typically require the numerical model to be reconstructed and the mesh to be redrawn whenever there are changes in the soil profiles or boundary conditions. This characteristic of PINNs can lead to more efficient and streamlined modeling processes. (c) Although both methods can be computationally intensive, PINNs can be more efficient in certain contexts. By embedding physical laws directly into the neural network architecture, PINNs can often reduce the dimensionality of the problem and exploit parallel computing resources more effectively. And, (d) PINNs have the potential for generalization and transfer learning, allowing models trained on one set of conditions to be adapted to new, similar problems with minimal retraining. This capability can

significantly reduce computational costs and time for new simulations.

The short-term excess PWP data, collected by monitoring sensors embedded in the ground, can be utilized to identify c_v with the assistance of PINNs. These embedded sensors, including piezometers and pore pressure gauges, offer advantages, such as real-time monitoring, the capability for long-term data collection, cost-effectiveness, and the preservation of in situ conditions. Upon identifying c_v, the prediction of excess PWP dissipation requires solving the partial differential equations (PDEs) for Terzaghi's consolidation theory. Contrary to traditional numerical methods for solving PDEs, PINNs afford several benefits: They facilitate the handling of complex geometries and boundaries without necessitating mesh generation, enable the seamless integration of observational or experimental data with the physics and mechanics described by the PDEs, and offer scalability and parallelization capabilities inherent to deep learning frameworks. Moreover, PINNs promote generalization and reusability, surpassing the specific cases for which they are initially trained, and diminish the requisite for a priori knowledge of the underlying physics and mechanics to shift the focus toward data-driven insights. Therefore, the combination of PINNs and monitoring sensors enhances the modeling process by providing real-time, high-resolution data that can be incorporated into the PINN framework. This approach circumvents the limitations associated with laboratory and in situ testing methods, as well as numerical simulations. These laboratory and in situ methods often face constraints related to the scale of experiments, environmental control, and the extensive time and resources required for comprehensive testing. By integrating sensor data, PINNs can achieve a more accurate and dynamic representation of soil consolidation behavior, thus overcoming these limitations. This synergistic use of sensors and PINNs ensures that the models are not only data driven but also capable of adapting to real-world conditions.

The proposed methodology utilizes a PINN to identify c_v from short-term excess PWP data collected by monitoring sensors embedded in stratified ground. Then, the identified c_v is employed to predict the long-term dissipation of excess PWP within the stratified ground, facilitating estimations of long-term ground settlement. Drawing upon a case study of a two-layer ground consolidation problem, strategic recommendations for sensor layout are proposed to optimize the monitoring of excess PWP. This research aims to provide an efficient approach to resolve issues related to stratified ground consolidation, capitalizing on the limited short-term data collected by monitoring sensors. Through this approach, enhancing the predictive accuracy and operational efficiency is sought in geotechnical engineering practices related to stratified ground consolidation.

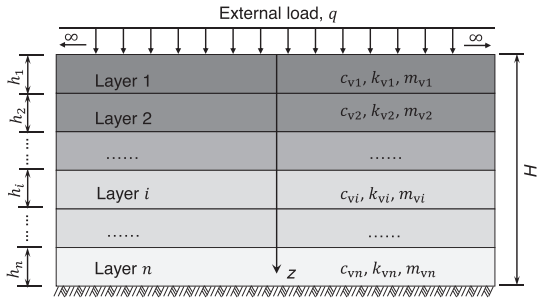

FIGURE 1 One-dimensional consolidation of stratified ground.

2 | PINN–TERZAGHI CONSOLIDATION THEORY FRAMEWORK

2.1 | Terzaghi consolidation theory

PINNs have gained successful applications to single-layer ground consolidation. For instance, Bekele (2021) and Yuan et al. (2024) used PINNs to solve one-dimensional (1D) and three-dimensional (3D) Terzaghi consolidation problems, respectively. Zhang et al. (2023) focused on characterizing and solving the 1D Terzaghi consolidation governing equations in conjunction with the measured data. In addition, Guo and Yin (2024) discretized the time to reduce the computational cost, which was validated in multidimensional forward and inverse problems. Compared to these single-layer ground models, stratified ground configurations offer a closer approximation to real-world conditions, as the Earth's subsurface is inherently stratified. Therefore, a stratified ground model is investigated in this study. Figure 1 shows a schematic of a stratified ground system. The consolidation equation applicable to stratified ground scenarios can be derived from the Terzaghi consolidation theory as:

$$c_{vi}\frac{\partial^2 u_i}{\partial z^2} = \frac{\partial u_i}{\partial t} \tag{1}$$

where u_i and c_{vi} represent the excess PWP and c_v of the ith (i.e., $i = 1, 2, 3, \ldots, n$) soil layer, respectively; z is the depth of soil element; and t is the time.

When solving the PDEs of Terzaghi's consolidation equation via PINNs, normalization plays a key role in enhancing both the network training process and performance. The rationale for implementing normalization includes (a) improving numerical stability by addressing issues that arise when handling variables across a

broad range of values; (b) enhancing the convergence of training by ensuring that the scale of the problem does not adversely affect gradient updates, thereby leading to more stable and efficient learning processes; (c) reducing training time due to enhanced numerical stability and improved convergence rates; (d) increasing model accuracy by preventing the undue influence of certain variables over others based solely on their scale; and (e) facilitating better generalization, thereby aiding the neural network in more effectively generalizing from the training data to unseen data. Consequently, the parameters involved in solving Equation (1) are normalized as follows:

$$\bar{z} = \frac{z}{z^*},\ \bar{t} = \frac{t}{t^*},\ \bar{u}_i = \frac{u_i}{u_0} \tag{2}$$

where z^* and t^* are the maximum depth and consolidation time of the stratified ground, respectively; and u_0 is the initial excess PWP. Through the normalization, all parameters are within the range from 0 to 1.

Substituting Equation (2) into Equation (1) yields the normalized form of the consolidation equation for the stratified ground:

$$\frac{\partial \bar{u}_i}{\partial \bar{t}} = \frac{c_{\mathrm{v}i} t^*}{z^{*2}} \frac{\partial^2 \bar{u}_i}{\partial \bar{z}^2} \tag{3}$$

Boundary and initial conditions are crucial for deriving the solution to a differential equation, especially within the context of PDEs. Boundary conditions define the behavior of a physical quantity at the domain limits. In the case of consolidation problems, boundary conditions are categorized as either drained or undrained. For the drained boundary condition, the excess PWP is set to zero, indicating that all pressure dissipates at the boundary:

$$\begin{cases} u\,(z=0,t)=0\,(\mathrm{Top}) \\ u\,(z=H,t)=0\ \ (\mathrm{Bottom}) \end{cases} \tag{4}$$

This boundary condition qualifies as a Dirichlet boundary condition, as it specifies the value of the function at the domain boundary.

For the undrained boundary condition, the gradient of excess PWP at the boundary is set to zero, indicating that there is no flow of pore water across the boundary:

$$\begin{cases} \dfrac{\partial u\,(z=0,t)}{\partial z} = 0\,(\mathrm{Top}) \\ \dfrac{\partial u\,(z=H,t)}{\partial z} = 0\,(\mathrm{Bottom}) \end{cases} \tag{5}$$

This boundary condition is classified as a Neumann boundary condition, as it specifies the value of the derivative of the function normal to the boundary.

The initial condition specifies the initial value of excess PWP at the onset of consolidation, u_0, which equals the external load, q, exerted on the ground surface:

$$u\ (z, t\ =\ 0) = u_0\ \ (z) =\ q \tag{6}$$

For stratified ground, it is essential to consider continuity conditions at the interface between soil layers. These conditions include the continuity of excess PWP and the continuity of flow across the stratified interface. This ensures that both the excess PWP and the pore water flow rate are consistent and uninterrupted at the interface separating different soil layers. Thus, the continuity conditions are written as:

$$\begin{cases} \left(k_{\mathrm{v}i}\dfrac{\partial u_i}{\partial z} - k_{\mathrm{v}(i+1)}\dfrac{\partial u_{i+1}}{\partial z}\right)_{z_{\mathrm{inter},i}} = 0 \\ (u_i - u_{i+1})_{z_{\mathrm{inter},i}} = 0 \end{cases} \tag{7}$$

where $k_{\mathrm{v}i}$ represents the vertical permeability coefficients of the ith soil layer; and $z_{\mathrm{inter},i}$ represents the depth of the stratified interface of the ith soil layer.

With the establishment of the initial condition (Equation (6)), boundary conditions (Equations (4) and (5)), and the equation that delineates the continuity conditions at the interfaces between soil layers (Equation (7)), the PDEs describing the consolidation process in stratified ground (Equation (3)) can be solved using PINNs, which will be demonstrated in the following sections.

2.2 | Physics-informed neural networks

PINNs constrain neural networks with the laws of physics and mechanics, which are articulated through PDEs. Instead of relying exclusively on extensive data sets for training, PINNs integrate these physical laws into the learning algorithm (Luo & Paal, 2023; Olivier et al., 2023). This integration allows PINNs to infer from significantly smaller data sets compared to conventional neural networks (Bui et al., 2020; Li et al., 2021, 2022). In addition, by embedding known physics into their structure, PINNs exhibit superior generalization capabilities beyond their training data sets, adhering to physical laws that enhance their robustness and reliability in prediction tasks (Cai et al., 2021; Karniadakis et al., 2021). To date, PINNs have been successfully employed in a variety of disciplines, including fluid dynamics (e.g., Kashefi & Mukerji, 2023; My Ha et al., 2022), heat transfer (e.g., Guo et al., 2023; Zobeiry & Humfeld, 2021), geophysics and geology (e.g., Almajid & Abu-Al-Saud, 2022; Liu et al., 2023), and energy systems (e.g., Huang & Wang, 2022; Ngo et al., 2024).

Given their effective framework for combining physical laws with data-driven insights, there exists considerable potential for PINNs to broaden their applications into an even wider array of fields (Chen et al., 2024; Nabian et al., 2021).

A PINN typically includes a neural network designed to predict solutions to specific PDEs. The training of this network focuses on minimizing a composite loss function, $\mathcal{L}$, which may comprise several components: (a) data loss, $\mathcal{L}_{\mathrm{D}}$, which quantifies the difference between the neural network predictions and the available observational or experimental data. This component is particularly relevant when training data extend beyond the constraints of physical laws; (b) physics-informed loss, $\mathcal{L}_{\mathrm{PDE}}$, also mentioned as the PDE residual, which measures the discrepancy in forecasts made by neural networks compared to the solutions described by the given PDEs; (c) boundary loss, $\mathcal{L}_{\mathrm{B}}$, ensuring that the neural network predictions adhere to the specified boundary conditions at the domain boundary; and (d) initial condition loss, $\mathcal{L}_{\mathrm{I}}$, guaranteeing that the network predictions at the initial time point are consistent with the stipulated initial conditions for time-dependent problems. Consequently, the overarching loss function for PINNs can be expressed as:

$$\mathcal{L} = \mathcal{L}_{\mathrm{D}} + \mathcal{L}_{\mathrm{PDE}} + \mathcal{L}_{\mathrm{B}} + \mathcal{L}_{\mathrm{I}} \tag{8}$$

Neural networks employ loss functions to quantify the inconsistency between the network prediction and the actual values. The loss function is pivotal in the training of neural networks, as it guides the model training by quantifying the network performance. It facilitates the backpropagation by enabling the neural network to learn through adjusting biases and weights to minimize the loss, and it also serves as a critical evaluation metric. In the computation of the loss function, a PINN utilizes automatic differentiation, a method distinguished by its precision and efficiency in calculating derivatives (Rall, 1981). This technique offers superior accuracy and computational efficiency compared to numerical differentiation and greater flexibility than symbolic differentiation (Baydin et al., 2018; Paszke et al., 2017). Automatic differentiation thus stands as a fundamental component in PINNs, facilitating the accurate incorporation of physical laws, expressed through PDEs, into the neural network learning process. This incorporation is crucial for ensuring that the neural network predictions are consistent with empirical data and conform to the underlying physical principles.

A neural network is comprised of multiple hidden layers, through which it propagates the inputs, X_j, and outputs, Y_j, where j denotes the layer number. The propagation process within each layer can be expressed as:

$$Y_j = \sigma_j \left(X_j w_j + b_j\right) \tag{9}$$

where b_j and w_j are the biases and weights, respectively; and σ_j is the activation function, commonly includes logistic function, Tanh function, and ReLU function. The parameters in Equation (9) can be optimized by minimizing the discrepancy measure, as outlined in Equation (8).

3 | PINNS FOR FORWARD AND INVERSE CONSOLIDATION PROBLEMS

3.1 | PINN framework for forward problem

In addressing the forward consolidation problem, where c_{v} is predetermined, the primary goal is to predict how excess PWP dissipates. The application of PINNs to resolve the forward consolidation problem within stratified ground acts as a pivotal assessment of PINN effectiveness. This methodology not only highlights the potential of PINNs in simulating complex consolidation processes but also establishes a framework for evaluating their ability to merge physical laws with computational intelligence for predictions in scenarios of stratified ground consolidation.

The framework of PINN developed for forward consolidation problem is depicted in Figure 2. It is structured as a fully connected neural network. The inputs include the spatial coordinate (z) and the time coordinate (t). At the initial output, the i th (i.e., $i = 1, 2, 3, \ldots, n$) soil layer corresponds to the i th excess PWP output, u_i. Subsequently, these n individual outputs are spliced in soil layer order to obtain the overall excess PWP output, u, for the stratified ground model. In this forward problem, the training of the PINN can be conducted without the need for supervised (observed) data. Thus, the data loss associated with the training process is nullified, that is, $\mathcal{L}_{\mathrm{D}} = 0$. Therefore, the PINN in the forward problem drives training through unsupervised data, which only includes the spatial coordinates (z) and the time coordinate (t) by introducing different loss functions.

The physics-informed loss, $\mathcal{L}_{\mathrm{PDE}}$, can be expressed as:

$$\mathcal{L}_{\mathrm{PDE}} = \lambda_{\mathrm{PDE}} \sum_{i=1}^{n} \left(\frac{\partial \bar{u}_i}{\partial \bar{t}} - \frac{c_{\mathrm{v}i} t^*}{z^{*2}} \frac{\partial^2 \bar{u}_i}{\partial \bar{z}^2} \right)^2 \tag{10}$$

where λ_{PDE} is the weight of the physics-informed loss.

The boundary loss, $\mathcal{L}_{\mathrm{B}}$, of the drained boundary is:

$$\mathcal{L}_{\mathrm{B}} = \begin{cases} \lambda_{\mathrm{B}} [u(z=0,t)]^2 \text{ (Top)} \\ \lambda_{\mathrm{B}} [u(z=H,t)]^2 \text{ (Bottom)} \end{cases} \tag{11}$$

where λ_{B} is the weight of the boundary loss.

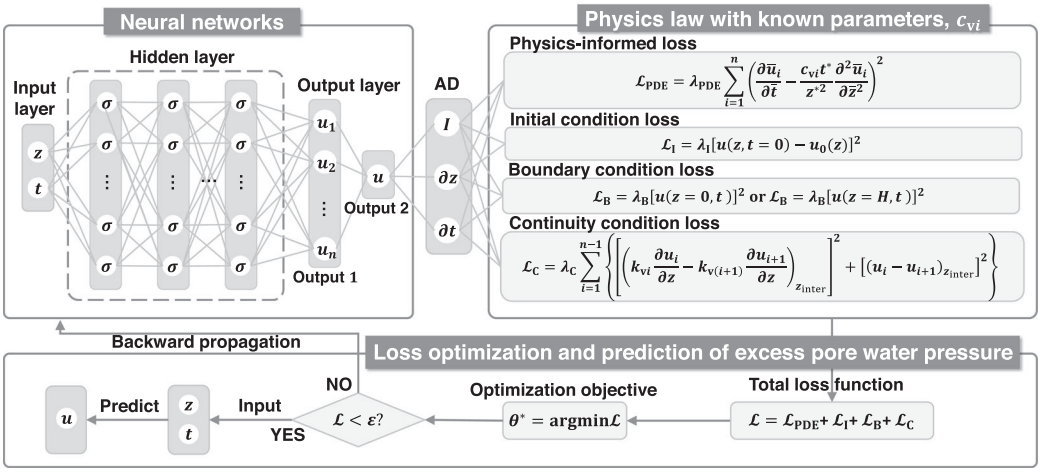

FIGURE 2 Physics-informed neural network (PINN) framework for solving forward consolidation problem in stratified ground (AD stands for automatic differentiation).

TABLE 1 All scenarios of total boundary loss.

Top surface	Bottom surface	Total boundary loss $\mathcal{L}_B^{\text{Total}}$
Drained	Drained	$\mathcal{L}_{\text{B}}^{\text{Total}} = \lambda_{\text{B}} \{[u(z = 0,t)]^2 + [u(z = H,t)]^2\}$
Undrained	Undrained	$\mathcal{L}_{\text{B}}^{\text{Total}} = \lambda_{\text{B}} \{[\frac{\partial u(z=0,t)}{\partial z}]^2 + [\frac{\partial u(z=H,t)}{\partial z}]^2\}$
Undrained	Drained	$\mathcal{L}_{\text{B}}^{\text{Total}} = \lambda_{\text{B}} \{[\frac{\partial u(z=0,t)}{\partial z}]^2 + [u(z = H,t)]^2\}$
Drained	Undrained	$\mathcal{L}_{\text{B}}^{\text{Total}} = \lambda_{\text{B}} \{[\frac{\partial u(z=H,t)}{\partial z}]^2 + [u(z = 0,t)]^2\}$

For the undrained boundary, the boundary loss, $\mathcal{L}_B$, should be written as:

$$\mathcal{L}_{\text{B}} = \begin{cases} \lambda_{\text{B}} \left[\dfrac{\partial u\,(z=0,t)}{\partial z}\right]^2 \text{(Top)} \\ \lambda_{\text{B}} \left[\dfrac{\partial u\,(z=H,t)}{\partial z}\right]^2 \text{(Bottom)} \end{cases} \tag{12}$$

The total boundary loss, $\mathcal{L}_{\text{B}}^{\text{Total}}$, of the top and bottom boundaries of stratified ground is calculated through the integration of Equation (11) and/or Equation (12), depending on the drainage characteristics. Table 1 lists all conceivable permutations of $\mathcal{L}_{\text{B}}^{\text{Total}}$, reflecting the varied configurations of drained or undrained condition of the stratified ground.

The initial condition loss, $\mathcal{L}_{\text{I}}$, is obtained from Equation (6) as:

$$\mathcal{L}_{\text{I}} = \lambda_{\text{I}} \left[u\,(z,t\ =\ 0) - u_0\,(z)\right]^2 \tag{13}$$

where λ_{I} is the weight of the initial condition loss.

In the context of stratified ground, it is imperative to account for the continuity of excess PWP and water flow across the interfaces of stratified soil layers. This consideration leads to the formulation of a loss term associated with the continuity condition as:

$$\mathcal{L}_{\text{C}} = \lambda_{\text{C}} \sum_{i\,=\,1}^{n-1} \left[\left(\left(k_{\text{v}i} \frac{\partial u_i}{\partial z} - k_{\text{v}(i+1)} \frac{\partial u_{i+1}}{\partial z} \right)_{z_{\text{inter},i}} \right)^2 + \left((u_i - u_{i+1})_{z_{\text{inter},i}} \right)^2 \right] \tag{14}$$

where λ_{C} is the weight of the continuity condition loss.

Consequently, the loss function for addressing the forward consolidation problem in stratified ground, $\mathcal{L}_{\text{Forward}}$, is formulated as:

$$\mathcal{L}_{\text{Forward}} = \mathcal{L}_{\text{C}} + \mathcal{L}_{\text{PDE}} + \mathcal{L}_{\text{B}}^{\text{Total}} + \mathcal{L}_{\text{I}} \tag{15}$$

3.2 | PINN framework for inverse problem

In previous PINN frameworks for consolidation problems (e.g., Guo & Yin, 2024), forward and inverse analyses are isolated from each other, and fail to utilize the inversion

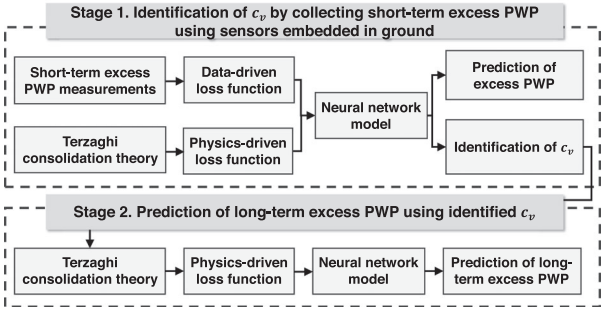

FIGURE 3 Physics-informed neural network (PINN) framework for solving inverse consolidation problem in stratified ground.

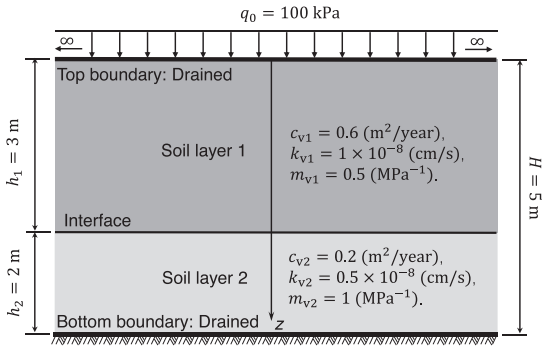

FIGURE 4 Two-layer ground consolidation problem.

parameters. In addition, random sampling of data over the full time period in the inverse problem ignores the issue of time efficiency in data collection. To overcome these challenges, the data collection strategy, that is, the monitoring sensor layout scheme, is optimized by exploring different factors, including sensor location and observation rate and period. More importantly, a PINN framework is proposed for the inverse problem to first identify c_v from the limited excess PWP data set and then utilizes the identified c_v to forward predict the long-term dissipation of excess PWP. This methodology leverages the collection of short-term excess PWP data to refine the long-term predictive analysis of ground consolidation. As a result, this methodology provides predictive insights into the long-term settlement of structures built on stratified ground, only based on short-term PWP observations.

Figure 3 shows the framework developed to tackle the inverse consolidation problem in stratified ground, which consists of two stages: stage 1 (the inverse model) and stage 2 (the forward model). The initial phase involves utilizing short-term measurements of excess PWP, collected via monitoring sensors, as the input for the PINN. These measurements form the basis for the PINN to identify c_v. Subsequently, this identified c_v is adopted to simulate and predict the long-term consolidation process of the stratified ground. The key difference between the inverse model and the forward model is the addition of a data-driven loss function and the inclusion of c_v as a trainable variable. The data-driven loss is calculated as:

$$\mathcal{L}_D = \lambda_D \left(u_i - u_i^{\text{Observed}}\right)^2 \tag{16}$$

where λ_D is the weight of the data loss; and u_i^{Obversed} is the observed excess PWP.

In the inverse model, each training iteration involves comparing the predicted excess PWP with the observed values and combining this comparison with the physics-driven loss function. Through this process, the PINN framework identifies c_v. The training log is monitored to track the identified c_v throughout the training process. The c_v value identified at the conclusion of the PINN training is considered the final identification result and is subsequently utilized for the long-term excess PWP prediction.

Consequently, the loss function for identifying c_v in the inverse model, $\mathcal{L}_{\text{Inverse}}$, is formulated as:

$$\mathcal{L}_{\text{Inverse}} = \mathcal{L}_D + \mathcal{L}_C + \mathcal{L}_{\text{PDE}} + \mathcal{L}_B^{\text{Total}} + \mathcal{L}_I \tag{17}$$

4 | CASE STUDY: TWO-LAYER GROUND CONSOLIDATION

4.1 | Case setting

A consolidation problem of the two-layer ground with the drained boundary at both the top and bottom surfaces is employed as a case to examine the validity of the proposed PINN method for predicting the consolidation of stratified ground. This case setting is shown in Figure 4. The soil thicknesses are 3 and 2 m, respectively. For the forward consolidation problem, c_v are known, which are 0.6 m^2/year and 0.15 m^2/year, respectively. The vertical permeability coefficients of the first and second soil layers are $k_{v1} = 1 \times 10^{-8}$ cm/s and $k_{v2} = 0.5 \times 10^{-8}$ cm/s, respectively. The external force exerted on the upper surface is $q_0 = 100$ kPa, which is equal to the initial excess PWP.

With these settings, the normalized PDEs of the consolidation problem of the two-layer ground are:

$$\begin{cases} \dfrac{\partial \bar{u}_1}{\partial \bar{t}} = \dfrac{c_{v1} t^*}{z^{*2}} \dfrac{\partial^2 \bar{u}_1}{\partial \bar{z}^2} \\ \dfrac{\partial \bar{u}_2}{\partial \bar{t}} = \dfrac{c_{v2} t^*}{z^{*2}} \dfrac{\partial^2 \bar{u}_2}{\partial \bar{z}^2} \end{cases} \tag{18}$$

The boundary conditions for the two-layer ground are:

$$\begin{cases} u_1|_{z=0\text{ m}} = 0 \\ u_2|_{z=5\text{ m}} = 0 \end{cases} \tag{19}$$

The initial condition is derived by equating the initial excess PWP to the external load:

$$u\ (z, t\ =\ 0) = q_0 \tag{20}$$

The continuity conditions between the two layers are:

$$\begin{cases} \left(k_{v1}\dfrac{\partial u_1}{\partial z} - k_{v2}\dfrac{\partial u_2}{\partial z}\right)_{z_{inter}=3m} = 0 \\ (u_1 - u_2)_{z_{inter}=3m} = 0 \end{cases} \tag{21}$$

For the consolidation problem of the two-layer ground, the analytical solutions can be found in Gray (1945). With the analytical solutions, the proposed PINN method can be evaluated by comparing the values obtained from the PINN to the values given by the analytical solutions. Two metrics, i.e., the absolute error, L_1, and relative error, L_2, are adopted:

$$L_1 = \left|y_i^{PINN} - y_i^{ANA}\right| \tag{22}$$

$$L_2 = \frac{\sqrt{\sum_i \left(y_i^{PINN} - y_i^{ANA}\right)^2}}{\sqrt{\sum_i \left(y_i^{ANA}\right)^2}} \tag{23}$$

where y_i^{PINN} and y_i^{ANA} are the values obtained from the proposed PINN method and the analytical solution, respectively. y_i denotes either excess PWP or c_v.

4.2 | Data set for model training and testing

For the forward problem, the training set was generated by sampling in the normalized spatio-temporal domain $\Omega \times \{\bar{z} \in [0,\ 1], \bar{t} \in [0,\ 1]\}$. These training points are referred to as unsupervised points (containing only temporal and spatial data and no excess PWP) and are used to compute the residuals of the loss functions. A larger number of these points is better for accuracy, but it also increases the computational burden (Nabian et al., 2021). To balance accuracy and efficiency, 10,000 points were generated by random sampling within this normalized spatio-temporal domain $\Omega \times \{\bar{z} \in (0, 1), \bar{t} \in (0, 1)\}$ to calculate the physics-informed loss. These points are not necessarily located on the interfaces between the soil layers, which is critical for calculating the continuity condition loss. To ensure that sufficient data points are available on the stratified interfaces for the continuity conditional loss calculation, an additional 200 points were supplemented. These 200 points were positioned by equidistant spacing specifically on the stratified interfaces to capture the continuity condition. For the boundary and initial condition losses, 1,000 points were randomly selected for each condition. In addition, to evaluate the proposed PINN prediction performance, 10,000 points generated equally spaced in the normalized spatio-temporal domain $\Omega \times \{\bar{z} \in [0,\ 1], \bar{t} \in [0,\ 1]\}$ were used as the testing set.

For the inverse problem, the training set differs in that, in addition to the unsupervised data described above, a small amount of supervised data (containing temporal and spatial data as well as excess PWP) needs to be introduced. The amount of these supervised data is related to the different monitoring sensor layout schemes, which will be presented in the subsequent sections.

4.3 | PINN hyperparameter optimization

In the development of PINNs, the determination of network hyperparameters is of paramount importance (Escapil-Inchauspé & Ruz, 2023; Kaplarević-Mališić et al., 2023). Hyperparameters include, but are not limited to, the hidden layer number, the number of neurons per layer, the learning rate, and the activation function selection. The influence of these hyperparameters on PINNs performance is multifaceted. For example, neuron networks with insufficient depth and neuron counts per layer may inadequately capture the complex physical laws governing the problem. Conversely, excessively large networks can lead to prolonged training durations, overfitting, and diminished generalization capabilities. Similarly, an overly aggressive learning rate might compromise the stability and convergence of the training process, while an overly conservative rate may unnecessarily extend it. The selection of activation functions also demands deliberate consideration, tailored to the task specifics.

Hyperparameter optimization can be approached through manual tuning or automated methods utilizing optimization algorithms. Manual tuning frequently meets the requisite accuracy standards (e.g., Bekele, 2021; Eusebi et al., 2024). In this study, a benchmark model comprising five layers with five neurons each and a learning rate of 0.01 was established. The Tanh function was employed as the activation function for the hidden layer due to its balanced output range and smooth derivatives, which can help improve convergence during training. The optimization of the loss function was handled by the adaptive moment estimation (Adam; Kingma & Ba, 2014), which demonstrates quicker convergence rates compared to alternative methods such as stochastic gradient descent (SGD; Bottou, 2010). Additionally, the Adam optimizer is more robust to the default values of hyperparameters than

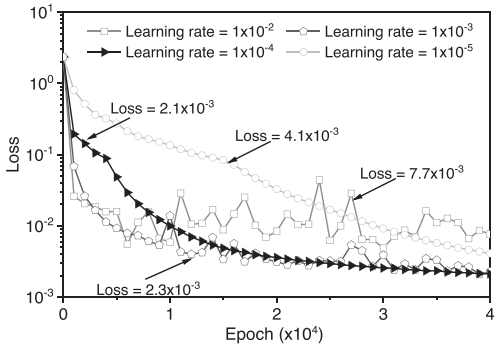

FIGURE 5 Training loss curves for the proposed physics-informed neural network (PINN) model with different learning rates.

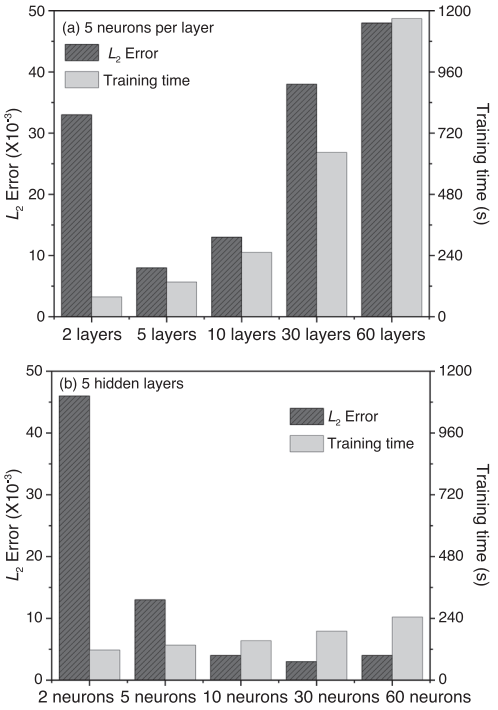

FIGURE 6 Training loss curves for the proposed physics-informed neural network (PINN) model: (a) varying numbers of hidden layers (5 neurons per layer) and (b) varying neurons per layer (5 hidden layers).

the SGD optimizer. For the normalized loss functions, a default weight configuration with all loss term weights set to 1 was adopted. This simplification proved effective for this study, contributing to stable and efficient training. Furthermore, this study compares the performance of various PINN configurations, adjusted through manual tuning, against this benchmark.

The proposed PINN was built in DeepXDE 1.11.0 (Karniadakis et al., 2021; Lu et al., 2021) and trained using TensorFlow 2.0 (Abadi, Agarwal, et al., 2016; Abadi, Barham, et al., 2016). The model training process ran on a Dell T7920 workstation, equipped with an NVIDIA GeForce RTX 3090 GPU and powered by an Intel(R) Xeon(R) Silver 4210R CPU at 2.4 GHz. It features 64 GB of RAM and 4 TB of hard disk storage. Initially, different learning rates were explored to assess their impact on the convergence of the proposed PINN. The primary objective of PINN training is to minimize the loss function. Consequently, the final loss value after training serves as a quantitative measure of convergence improvement. Figure 5 shows that a learning rate of 1×10^{-2} results in significant oscillations in the loss curve. As the learning rate decreases, the training curve becomes smoother, and convergence improves. At a learning rate of 1×10^{-4}, the total loss value is minimized, indicating optimal convergence. Although a learning rate of 1×10^{-5} enhances training stability, the initial loss reduction is slow, which is detrimental to model convergence, and more training epochs are needed to further improve the convergence. Therefore, a learning rate of 1×10^{-4} was selected for the proposed PINN model.

The impact of changing the hidden layer numbers and the neuron numbers per hidden layer on how the proposed PINN perform was examined. Models featuring 2, 5, 10, 30, and 60 hidden layers, each with 5 neurons, were developed to investigate the influence of hidden layer quantity. Figure 6a shows that training time increases with increasing the number of hidden layers; however, prediction accuracy does not exhibit a consistent upward trajectory. The benchmark model achieved the lowest L_2 error among the configurations tested, indicating that reducing the number of hidden layers may lead to inadequate model representation and underfitting. Conversely, an excessive number of hidden layers exacerbates the nonconvergence effect, leading to gradient explosion at high learning rates and gradient vanishing at low learning rates. Besides, it prolongs the training time.

To assess the effect of neuron density, PINN models with 2, 5, 10, 30, and 60 neurons in each hidden layer, while maintaining a five-layer structure, were constructed. Figure 6b shows that the model with 30 neurons per layer exhibited the lowest L_2 error and a shorter training duration compared to the model with 60 neurons per layer. It also maintained a reasonable training time when compared to models with 2 and 5 neurons per layer, thus striking an optimal balance between complexity and efficiency.

Through the manual tuning analysis described above, the optimally configured PINN features five hidden layers and each hidden layer composed of 30 neurons. The learning rate is fixed at 1×10^{-4}, the activation method is the Tanh function, and the optimization algorithm adopted is Adam.

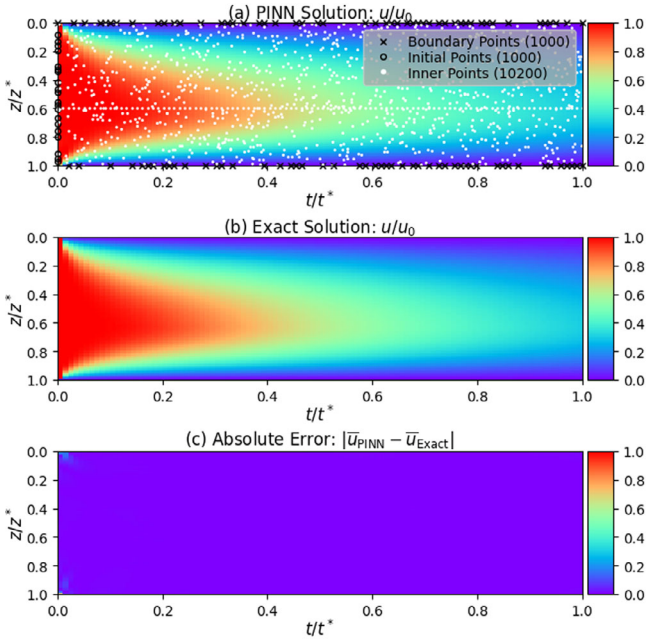

FIGURE 7 Two-dimensional (2D) maps of dissipation of excess pore water pressure (PWP) predicted by (a) tuned physics-informed neural network (PINN), (b) analytical solution, and (c) 2D map of absolute error, L_1. (The white points, black hollow points, and x-marked points shown in (a) are the training set. Not all of them are displayed due to their large number.)

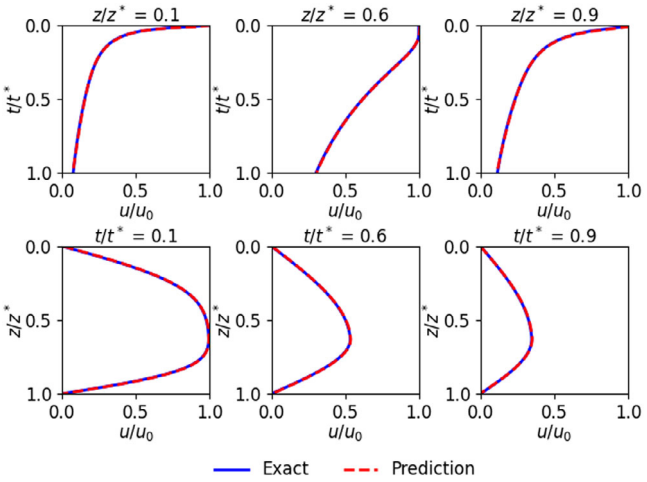

FIGURE 8 Comparison of physics-informed neural network (PINN) predictions and analytical solutions at various moments and locations.

4.4 | Forward problem: Prediction of excess PWP

The prediction of excess PWP of the two-layer ground consolidation for 10 years was conducted using the tuned PINN and the analytical solution. It is observed that the 2D maps showing the dissipation of excess PWP obtained by the PINN (Figure 7a) and the analytical solution (Figure 7b) are almost identical. This is also demonstrated in Figure 7c, where the absolute error, L_1, at every location in the 2D map is zero, except at the positions of the upper and lower boundaries at the initial moment. The nonzero errors at these positions may result from conflicts between the boundary and initial conditions, rather than inaccuracies in the PINN model. At the initial moment, the excess PWP at any position of the ground is the external load, while at the drainage boundary, the excess PWP is set to zero. Thus, at the initial moment, there is a conflict between the excess PWP at the upper and lower boundary positions. Although this conflict is unavoidable, it has minimal influence on the long-term prediction of excess PWP as it only affects the upper and lower boundaries at the initial moment. In addition, Figure 8 compares the PINN prediction and the analytical solution at different moments and locations. It is observed that all the predicted curves by the PINN and the analytical solution coincided with each other. Thus, the efficacy of the proposed PINN for solving consolidation problems of stratified ground is demonstrated.

4.5 | Effects of sensor layout on inverse results

To assess the impact of monitoring sensor layouts on the PINN inverse results, two to four monitoring sensors are employed. The sensors were positioned at either equal intervals or various depths throughout the soil profile, as shown in Figure 9. The sensors conducted 100 observations at a frequency of once every 0.01 years. These observations are the supervised training sets for the inversion model. This observation frequency was arbitrarily chosen, and its implications will be examined in the following section. In this analysis, control variables are introduced to underscore the importance of the burial depths of the sensors.

Figure 10 shows the identification results for c_v alongside the corresponding errors. When two monitoring sensors are positioned at varying depths, specifically where the excess PWP undergoes significant changes, the identification results for c_v most closely align with the actual values, evidenced by the errors of 0.005 for both c_{v1} and c_{v2}. Conversely, positioning the sensors at equal intervals leads to the diminished identification accuracy. Specifically, the identification accuracy of c_{v1} is lowest (0.013) when utilizing two or three sensors at equal distances. This minimum accuracy is attributed to these sensors being placed at locations where the excess PWP is least variable. The accuracy improves when four sensors are used at equal distances, due to the positioning of the first-row sensor in the

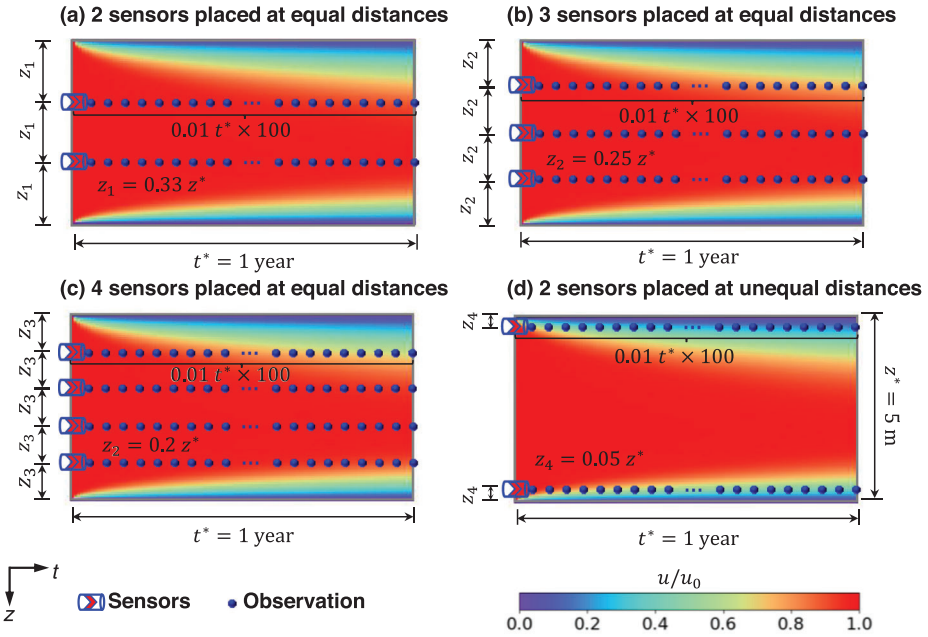

FIGURE 9 Schematic of sensor layout in the two-layer ground.

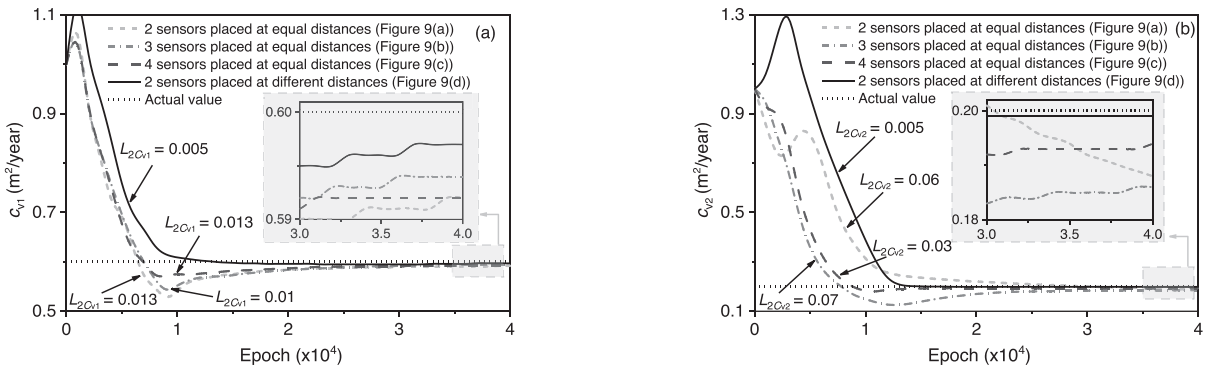

FIGURE 10 Identification of c_v using different sensor layouts: (a) c_{v1} and (b) c_{v2} (the identification value is saved every 1000 epochs of training, and the last identification value is taken as the final result and used to calculate the relative error).

four-sensor layout being closer to the location of the high PWP variability. However, for the identification of c_{v2}, performance with two, three, or four sensors placed at equal intervals is all suboptimal. This is because the sensors in the last row are positioned far from the position with the significant excess PWP variability in the second soil layer.

These different identification results of c_v highlight the importance of prior knowledge for monitoring sensor layout. According to consolidation theory, significant spatial changes in excess PWP are associated with boundary conditions. Water in the soil layer is discharged through the permeable boundary, leading to the dissipation of excess PWP. Consequently, near the permeable boundary, the excess PWP will undergo significant spatial changes. Therefore, for accurate identification of c_v, it is recommended to position monitoring sensors in proximity to the permeable boundary.

4.6 | Effects of sensor observation period and rate on inverse results

The effects of various sensor observation periods and rates on the identification results of c_v were investigated to find the optimal observation period and rate. First, the sensor observations were conducted for 0.01-year, 0.03-year, and 0.05-year periods at a rate of 0.01 year to produce an observation (see Figure 11a–c). Figure 12a,b shows that the identification errors for c_{v1} and c_{v2} decrease with an increase in the sensor observation period, which indicates

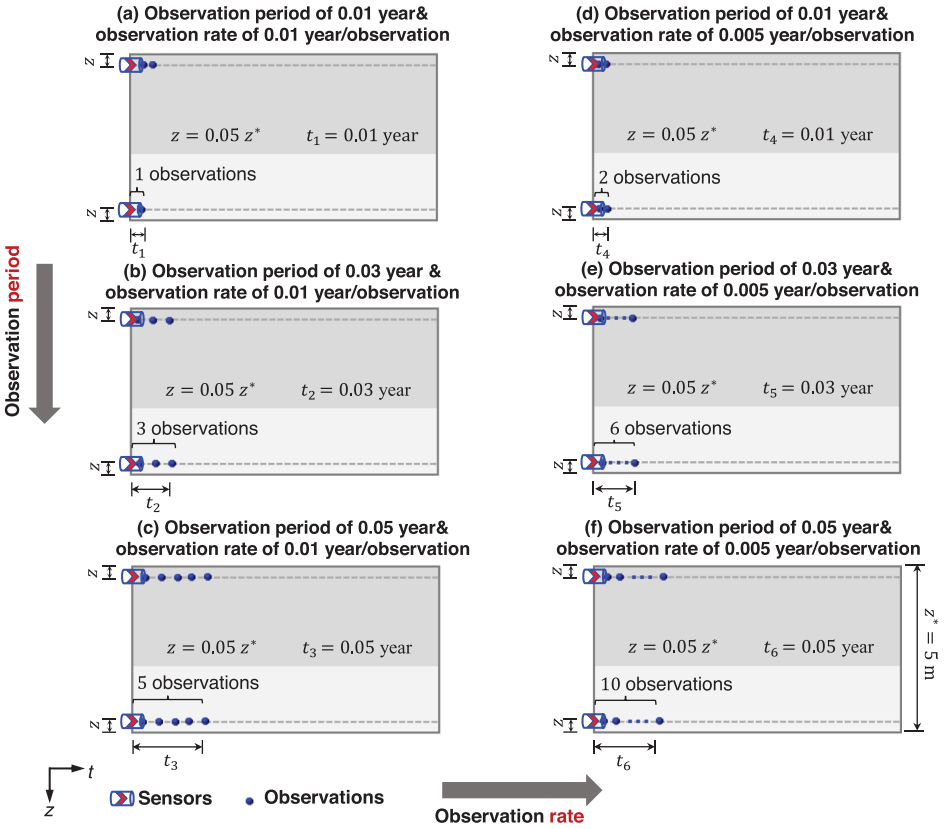

FIGURE 11 Schematic of different observation periods and rates.

that the identification accuracy of c_v is affected by the observation period. The longer the observation period, the higher the identification accuracy. However, the optimization goal of the sensor layout is to achieve the best performance at the lowest cost (Gutierrez Soto & Adeli, 2013). If shorter observation periods yield good results, this can save time and increase the efficiency of the predictions.

The identification error for c_{v1} consistently remains lower than that of c_{v2} across all three observation periods. This difference might be attributed to the variance in excess PWP across different soil layers, since c_{v1} and c_{v2} were identified based on the excess PWP data. In particular, the variation in excess PWP is more pronounced in the first soil layer than in the second.

Besides, the impacts of increased data density resulting from higher sensor observation rates on the identification accuracy of c_v under these three observation period conditions are explored (Figure 11d–f). Figure 12 shows that with the observation periods of 0.01 year and the observation rate of 0.005 year/observation, although the observation rate is increased, the identification errors of c_{v1} and c_{v2} were still high. However, for the 0.05-year observation period, the identification error of c_{v2} decreases from 0.03 to 0.025 by increasing the observation rate, but the identification error of c_{v1} does not change significantly as the error of 0.01 year/observation is already small. This implies that within a specific observation period, increasing observation data density through a faster observation rate can enhance the identification accuracy.

From the above analyses, it is evident that with an observation period of 0.05 years and an observation rate of 0.005 years per observation, the proposed PINN can achieve high identification accuracy for c_v.

4.7 | Inverse problem: Identification of c_v and subsequent prediction of excess PWP

The parameters employed for solving the inverse problem are identical to those used in addressing the forward problem for the consolidation of the two-layer ground. The sole distinction lies in c_v being undefined, necessitating its back-calculation through the application of the PINN and the short-term monitoring of excess PWP. Unlike the forward prediction of excess PWP where c_v are known, it is essential to leverage supervised data to establish a constraint for identifying c_v in the inverse problem.

To identify c_v for the first and second layers of the ground, a 0.05-year observation period of excess PWP is utilized. Twenty data points of excess PWP, measured at depths $z_1 = 0.25$ m and $z_2 = 4.75$ m (i.e., the monitoring sensor location), respectively, act as the supervised data.

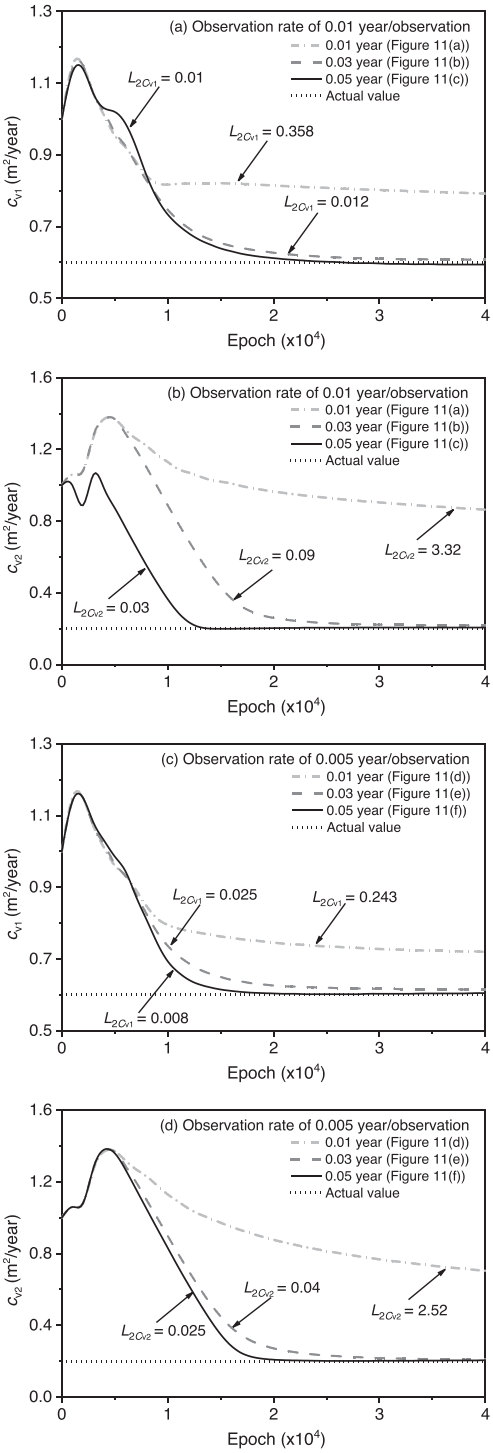

FIGURE 12 Identification of c_v using different observation periods and rates: (a, b) c_{v1} and c_{v2} using observations with observation rate of 0.01 year/observation; and (c, d) c_{v1} and c_{v2} using observations with observation rate of 0.005 year/observation.

The sensor layout setting has been demonstrated optimal in the previous sections. Figure 13 shows the identification results for c_v, with c_{v1} equal to 0.605 m^2/year and c_{v2} equal to 0.205 m^2/year. It is observed that the identified c_v align closely with the actual values, and the L_2 errors are

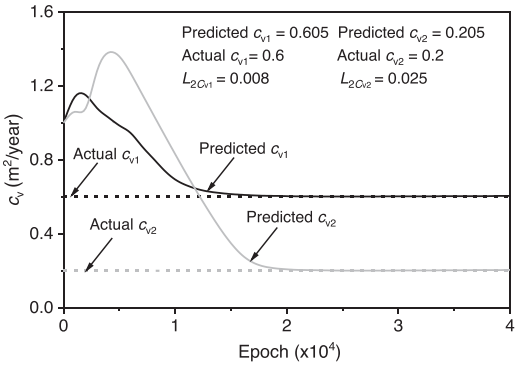

FIGURE 13 Identification of c_v using the proposed physics-informed neural network (PINN) and short-term monitoring of excess pore water pressure (PWP).

0.008 and 0.025, respectively. These small errors validate that the identification results obtained through the PINN accurately match the actual values.

The identified c_v were utilized to predict the excess PWP at intervals of 1 year, 10 years, 15 years, and 30 years. Figure 14 presents the prediction outcomes for excess PWP over these timeframes. The use of the identified c_v facilitates accurate predictions of excess PWP. This accuracy is evidenced by the nearly identical 2D maps of excess PWP produced by the PINN and the analytical solution. The near-zero absolute errors on the 2D maps at various intervals further support this. An increase in the dissipation time from 1 to 30 years leads to a slight increase in L_2 errors, indicating a decrease in prediction accuracy over time. Despite this, the prediction accuracy remains acceptable at 30 years, with an L_2 error of only 0.01.

5 | VALIDATION

5.1 | Comparison with an existing method

To further demonstrate the validity and novelty, the proposed PINN method is compared with an existing PINN method (Bekele, 2021) and a laboratory oedometer test for a two-layer system (Chai et al., 2009).

The double-layer ground case is degraded to a single-layer ground case for comparison with an existing method (Bekele, 2021). The top and bottom boundary conditions of the ground are pervious. The layer depth is 5 m. An external force of 100 kPa is applied to the upper surface of the ground. c_v and k_v were chosen to be 0.2 m^2/year and 0.5×10^{-8} cm/s, respectively.

Previous studies (Bekele, 2021; Guo & Yin, 2024; Zhang et al., 2023) utilized random and uniform sampling methods to generate supervised data within the spatio-temporal

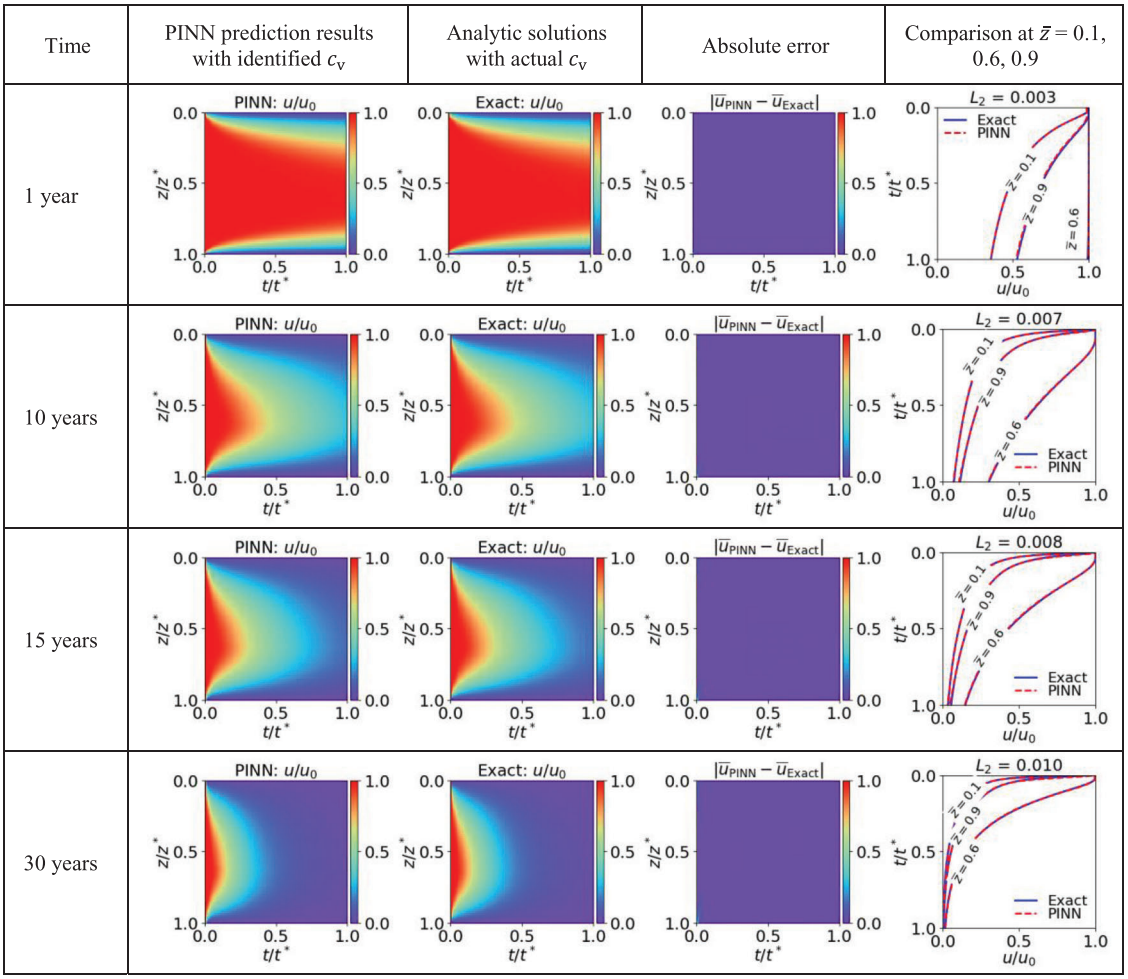

FIGURE 14 Comparison of long-term excess pore water pressure (PWP) predictions: Physics-informed neural network (PINN) with identified c_v versus analytical solution.

domain. In contrast, a novel strategy for collecting observation points by positioning sensors in near the permeable boundary and initiating monitoring at time zero was adopted. Using the proposed sampling strategy, 10 supervised datapoints were generated isometrically in the normalized spatio-temporal $\Omega \times \{\bar{z} = 0.05, \bar{t} \in [0,\ 0.05]\}$. Referring to Bekele (2021), 2,000 supervised data were randomly generated in the normalized spatio-temporal domain $\Omega \times \{\bar{z} \in [0,\ 1], \bar{t} \in [0,\ 1]\}$. Both sets of cases maintained consistency with the two-layer case in terms of unsupervised configurations and model parameter settings, except for the exclusion of unsupervised points used to compute layered interface losses.

Figure 15 presents the identification outcomes for c_v using different supervised data sets. The identified c_v trained on 10 supervised datapoints collected by the proposed method is 0.201 m^2/year with an L_2 error of 0.005, which is more accurate than the result of 0.197 m^2/year for the random sampling of 2,000 supervised data in the Bekele's work. It is noteworthy that the random sampling method requires assuming all analytical solutions

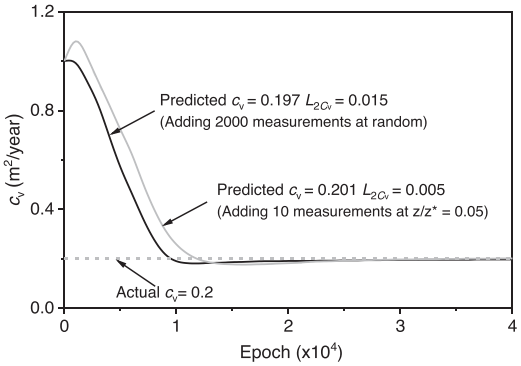

FIGURE 15 Identification of c_v in single-layer ground using the proposed and existing physics-informed neural network (PINN) methods.

are known across the spatio-temporal domain, implying that sensors would need to gather data for an entire year, thereby incurring significant temporal costs. However, by positioning sensors near the permeable boundary and initiating monitoring at time zero, data collection

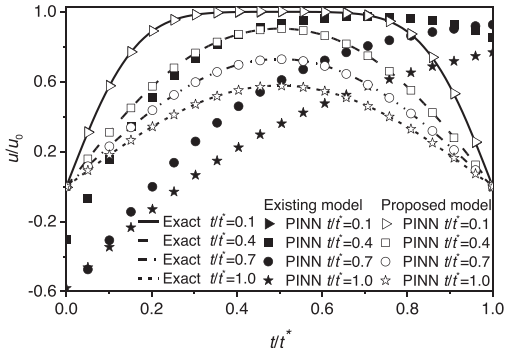

FIGURE 16 Comparison of proposed physics-informed neural network (PINN) predictions and existing PINN predictions at various moments.

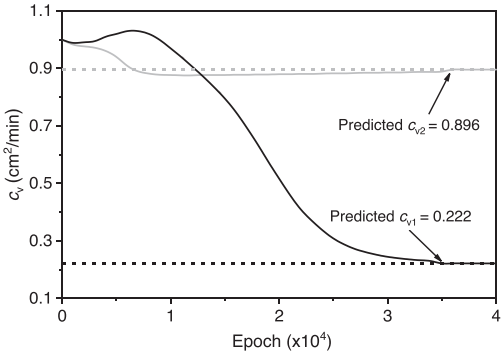

FIGURE 17 Identification of c_v using the proposed physics-informed neural network (PINN) method with the first 100 min monitoring of excess pore water pressure (PWP).

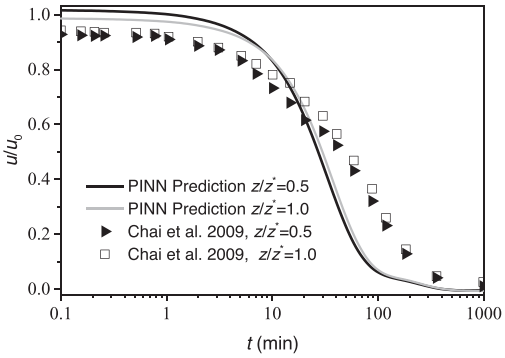

FIGURE 18 Comparison of physics-informed neural network (PINN) predictions with identified c_v and test measurements at various moments.

can be limited to just 0.05 years, substantially reducing observational expenses.

In the process of using supervised data to identify c_v, the trained model can directly predict the excess PWP, as demonstrated in Bekele's research and corresponding to the first stage of Figure 3. This model, along with the proposed PINN model, is utilized to predict the excess PWP of the single-layer ground at 1 year, 4 years, 7 years, and 10 years, respectively. Figure 16 presents the excess PWP prediction results of the proposed and existing PINN methods at different moments. Both the existing and proposed PINN models provide predictions of the excess PWP at 1 year that are relatively close to the analytical solution. As time progresses, the discrepancy between the predicted values of the existing model and the analytical solution gradually increases, with significant errors appearing when predicting the excess PWP at 10 years. In contrast, the proposed PINN model continues to exhibit good predictive performance in the long-term prediction of excess PWP.

5.2 | Comparison with an oedometer test

A laboratory oedometer test for a two-layer system with both surcharge load and vacuum pressure were carried out by Chai et al. (2009). The test case with the top drained boundary under surcharge load was employed to validate the efficiency of the proposed PINN method in real situation. The vertical permeability coefficients of the two soils layers are 1.44×10^{-9} m/s and 3.13×10^{-9} m/s, respectively. Each soil layer has a thickness of 20 mm. At the initial moment, an external force q_0 (= 80 kPa) is applied at the top of different soil layers.

For the identification of c_v, the 44 measured excess PWP data recorded at the bottoms of layer 1 and layer 2 during the first 100 min were utilized as supervised data. Other parameters, such as unsupervised points and model settings, are consistent with the previous two-layer ground simulation cases. The identification results for c_v are shown in Figure 17. After 40,000 training epochs, the identified c_{v1} and c_{v2} converged to 0.222 cm^2/min and 0.896 cm^2/min, respectively. These identified c_v values were subsequently utilized to predict the excess PWP over 1,000 min. Figure 18 presents the prediction outcomes for excess PWP at the bottom of the different soil layers. It is observed that the predicted values align closely with the actual values, with an L_2 error of 0.117. The small error validates the potential of the proposed PINN model for practical applications.

6 | NOISE SENSITIVITY ANALYSIS

To validate the robustness of the proposed method, an approach by adding Gaussian noise to the analytical data is adopted. This approach simulates the variability and unpredictability typically observed in real ground monitoring scenarios.

Varying levels of random Gaussian noise (with a mean of zero and standard deviation corresponding to the noise

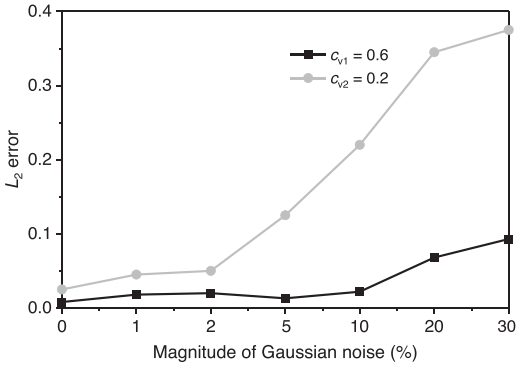

FIGURE 19 Identification error of c_v with different Gaussian noise levels.

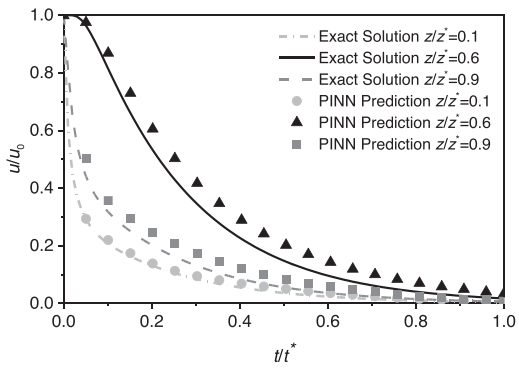

FIGURE 20 Comparison of physics-informed neural network (PINN) predictions with identified c_v and analytical solutions at various locations.

level) are introduced into the 0.05-year sensor monitoring data set comprising 20 data points. Figure 19 shows the identification results with the inclusion of various levels of noises. The introduction of noise degrades the identification accuracy of both c_{v1} and c_{v2} compared to the original data without noise interference. c_{v2} has a higher sensitivity to noise, and its identification error shows a significant increase with the increase of noise level, which may be ascribed to the insignificant change of excess PWP in the second soil layer. However, at 2% noise level, the identification results of c_{v1} and c_{v2} are within a small error as the error values are 0.02 and 0.05, respectively. Note that there are a few cases (such as at 5% noise) that do not follow this trend that the inversion error increases with the noise level, which may be due to stochastic effects. A similar phenomenon has also been observed in the study by Guo et al. (2023).

The identified c_{v1} (= 0.587) and c_{v2} (= 0.156) from the data with 10% noise level were utilized to predict the 30-year excess PWP. Figure 20 shows the prediction outcomes for excess PWP at various locations. The predicted excess PWP at locations close to the second layer sensor ($z/z^* =$ 0.9) and at the layered interfaces ($z/z^* =$ 0.6) deviates somewhat from the analytical solution. This is caused by the large identification error (= 0.216) of c_{v2}, which is attributed to the less significant variation of excess PWP in the second layer. However, the predictions at locations closer to the first layer sensor ($z/z^* =$ 0.1) are in general agreement with the analytical solution. Note that although PINN is sensitive to low excess PWP variations, this can be mitigated by increasing the observation period to observe larger changes in excess PWP.

7 | CONCLUSION

A PINN-based methodology that utilizes short-term excess PWP monitoring data to identify coefficients of consolidation and predict the long-term consolidation process of stratified ground was proposed. Frameworks to solve both forward and inverse consolidation problems for stratified ground and predict the long-term dissipation of excess PWP in stratified ground were developed. The validity of the proposed PINN methodology in addressing stratified ground consolidation challenges was demonstrated through a case study involving a two-layer ground consolidation problem, with comparisons made to an existing PINN method and a laboratory oedometer test for a two-layer system. To identify the optimal neural network configuration, a manual tuning approach was employed by comparing various learning rates, hidden layer numbers, and neuron counts per layer. This tuning process resulted in the adoption of a 5-hidden-layer neural network, each layer comprising 30 neurons, and a learning rate of 1×10^{-4}. With this optimized PINN, both forward and inverse problems of the two-layer ground consolidation problem were solved. Moreover, the optimal layout for monitoring sensors was explored and the effects of sensor observation period and rate were investigated. The key conclusions from this study are outlined below:

(a) The proposed PINN methodology demonstrated robust performance in solving forward and inverse consolidation problems related to stratified ground. For a 5-m-deep, two-layer ground, it achieved accurate predictions of the 10-year excess PWP dissipation in the forward scenario and by leveraging a mere 0.05-year sensor monitoring data set comprising only 20 data points, it identified c_v and extended its predictive accuracy to the 30-year excess PWP dissipation.
(b) PWP monitoring sensors should be installed in areas experiencing significant variations in excess PWP to ensure the optimal performance of the proposed PINN methodology. In addition, the proposed PINN method

can attain high precision in c_v identification when the noise level is maintained within 2%.

(c) The proposed PINN methodology exhibits potential for predicting the consolidation of stratified ground, necessitating only short-term PWP monitoring data with a few data points. This advantage positions the method favorably against laboratory-empirical approaches, numerical simulations, and in situ testing methods due to its real-time monitoring capacity, cost-effectiveness, and ability to preserve in situ conditions, reduced time consumption, and enhanced generalization capabilities.

It is acknowledged that the proposed methodology also has some limitations, including (i) when the number of soil layers increases or when there is spatial heterogeneity in soil parameters, the complexity of the problem increases significantly. This could potentially affect the accuracy and efficiency of the proposed method due to the increased computational demand and the need for advanced modeling techniques to capture the heterogeneous properties of the soil. And, (ii) the proposed methodology is sensitive to noise at low excess PWP variations. However, the proposed layout scheme for monitoring sensors is expected to remain valid, as it captures significant variations in excess PWP. Accurately capturing these variations will enhance the prediction accuracy of the proposed methodology.

To address these limitations, future research will focus on the scalability of the proposed methodology to heterogeneous soil profiles and evaluating its performance under varying boundary conditions or loading scenarios. Probabilistic methods will be developed to incorporate uncertainty variations, enhancing robustness and reliability in practical applications. More techniques of imposing boundary conditions, such as hard constraints, will be investigated to flexibly cope with complex and conflicting boundary conditions. Machine learning algorithms will be employed to optimize sensor placement (Sajedi & Liang, 2022) to reduce maintenance costs and will be applied to the development of smart sensors (Amezquita-Sanchez et al., 2018; Naderpoor Shad & Taghikhany, 2022) to automate data monitoring, parameter identification, and prediction. Furthermore, other novel machine learning algorithms will be explored as alternative approaches and research extensions, including neural dynamic classification algorithm (Rafiei & Adeli, 2017), dynamic ensemble learning algorithm (Alam et al., 2020), finite element machines for fast learning (Pereira et al., 2020), and self-supervised learning (Rafiei et al., 2022).

ACKNOWLEDGMENTS

The authors from Chang'an University acknowledge the financial support offered by the National Natural Science Foundation of China (grant number 52108297), the Postdoctoral Research Foundation of China (grant number 2021M692742), the Special Support Project of the China Postdoctoral Science Foundation (grant number 2023T160560), the Qin Chuang Yuan Imported High-level Innovation and Entrepreneurship Talent Project (grant number OCYRCXM-2022-29), and the Fundamental Research Funds for the Central Universities, CHD (grant number 300102212301). It should be noted that Weibing Gong from Missouri S&T has not received any financial support from the aforementioned funding sources.

REFERENCES

Abadi, M., Agarwal, A., Barham, P., Brevdo, E., Chen, Z., Citro, C., Corrado, G. S., Davis, A., Dean, J., Devin, M., Jia, Y., Jozefowicz, R., Kaiser, L., Kudlur, M., Levenberg, J., Mane, D., Monga, R., Moore, S., Murray, D., … Zheng, X. (2016). Tensorflow: Large-scale machine learning on heterogeneous distributed systems, arXiv preprint:1603.04467.

Abadi, M., Barham, P., Chen, J., Chen, Z., Davis, A., Dean, J., Devin, M., Ghemawat, S., Irving, G., Isard, M., Kudlur, M., Levenberg, J., Monga, R., Moore, S., Murray, D. G., Steiner, B., Tucker, P., Vasudevan, V., Warden, P., … Zheng, X. (2016). {Tensorflow}: A system for {large-scale} machine learning. In 12th USENIX symposium on operating systems design and implementation (OSDI 16) (pp. 265–283), USENIX Association.

Abbasi, N., Rahimi, H., Javadi, A. A., & Fakher, A. (2007). Finite difference approach for consolidation with variable compressibility and permeability. *Computers and Geotechnics*, *34*(1), 41–52.

Alam, K. M. R., Siddique, N., & Adeli, H. (2020). A dynamic ensemble learning algorithm for neural networks. *Neural Computing and Applications*, *32*(12), 8675–8690.

Almajid, M. M., & Abu-Al-Saud, M. O. (2022). Prediction of porous media fluid flow using physics informed neural networks. *Journal of Petroleum Science and Engineering*, *208*, 109205.

Alzubaidi, R. (2020). Effect rate of strain on in situ horizontal coefficient of consolidation from pressuremeter. *Geotechnical and Geological Engineering*, *38*, 1669–1674.

Amezquita-Sanchez, J. P., Valtierra-Rodriguez, M., & Adeli, H. (2018). Wireless smart sensors for monitoring the health condition of civil infrastructure. *Scientia Iranica-A*, *25*(6), 2913–2925.

Baydin, A. G., Pearlmutter, B. A., Radul, A. A., & Siskind, J. M. (2018). Automatic differentiation in machine learning: A survey. *Journal of Machine Learning Research*, *18*(153), 1–43.

Bekele, Y. W. (2021). Physics-informed deep learning for one-dimensional consolidation. *Journal of Rock Mechanics and Geotechnical Engineering*, *13*(2), 420–430.

Bottou, L. (2010). Large-scale machine learning with stochastic gradient descent. In *Proceedings of COMPSTAT 2010: 19th international conference on computational statistics* (pp. 177–186), Paris France, August 22–27, 2010. Springer.

Bui, D. T., Tsangaratos, P., Nguyen, V.-T., Van Liem, N., & Trinh, P. T. (2020). Comparing the prediction performance of a deep learning neural network model with conventional machine learning models in landslide susceptibility assessment. *Catena*, *188*, 104426.

Cai, S., Mao, Z., Wang, Z., Yin, M., & Karniadakis, G. E. (2021). Physics-informed neural networks (PINNs) for fluid mechanics: a review. *Acta Mechanica Sinica*, *37*(12), 1727–1738.

Cargill, K. W. (1984). Prediction of consolidation of very soft soil. *Journal of Geotechnical Engineering*, *110*(6), 775–795.

Chai, J. C., Matsunaga, K., Sakai, A., & Hayashi, S. (2009). Comparison of vacuum consolidation with surcharge load induced consolidation of a two-layer system. *Géotechnique*, *59*(7), 637–641.

Chen, S. Z., Feng, D. C., & Taciroglu, E. (2024). Prior knowledge-infused neural network for efficient performance assessment of structures through few-shot incremental learning. *Computer-Aided Civil and Infrastructure Engineering*, *39*(13), 1928–1945.

Chiou, Y. J., & Chi, S. Y. (1994). Boundary element analysis of Biot consolidation in layered elastic soils. *International Journal for Numerical and Analytical Methods in Geomechanics*, *18*(6), 377–396.

Clarke, B. (1990). Consolidation characteristics of clays from self-boring pressuremeter tests, Geological Society, London. *Engineering Geology Special Publications*, *6*(1), 33–37.

Duncan, J. M. (1993). Limitations of conventional analysis of consolidation settlement. *Journal of Geotechnical Engineering*, *119*(9), 1333–1359.

Escapil-Inchauspé, P., & Ruz, G. A. (2023). Hyper-parameter tuning of physics-informed neural networks: Application to Helmholtz problems. *Neurocomputing*, *561*, 126826.

Eusebi, R., Vecchi, G. A., Lai, C. Y., & Tong, M. (2024). Realistic tropical cyclone wind and pressure fields can be reconstructed from sparse data using deep learning. *Communications Earth & Environment*, *5*(1), 8.

Gong, W., Li, J., Li, L., & Zhang, S. (2017). Evolution of mechanical properties of soils subsequent to a pile jacked in natural saturated clays. *Ocean Engineering*, *136*, 209–217.

Gong, W., Li, L., Zhang, S., & Li, J. (2020). Long-term setup of a displacement pile in clay: an analytical framework. *Ocean Engineering*, *218*, 108143.

Gray, H. (1945). *Simultaneous consolidation of contiguous layers of unlike compressible soils*, American Society of Civil Engineers, 110, 1327–1344.

Guo, H., & Yin, Z. Y. (2024). A novel physics-informed deep learning strategy with local time-updating discrete scheme for multi-dimensional forward and inverse consolidation problems. *Computer Methods in Applied Mechanics and Engineering*, *421*, 116819.

Guo, H., Zhuang, X., Fu, X., Zhu, Y., & Rabczuk, T. (2023). Physics-informed deep learning for three-dimensional transient heat transfer analysis of functionally graded materials. *Computational Mechanics*, *72*(3), 513–524.

Holtz, R. D., Kovacs, W. D., & Sheahan, T. C. (2011). *An introduction to geotechnical engineering* (2nd ed.). Prentice-Hall.

Horpibulsuk, S., Chinkulkijniwat, A., Cholphatsorn, A., Suebsuk, J., & Liu, M. D. (2012). Consolidation behavior of soil–cement column improved ground. *Computers and Geotechnics*, *43*, 37–50.

Huang, B., & Wang, J. (2022). Applications of physics-informed neural networks in power systems—A review. *IEEE Transactions on Power Systems*, *38*(1), 572–588.

Jang, I. S., Chung, C.-K., Kim, M. M., & Cho, S. M. (2003). Numerical assessment on the consolidation characteristics of clays from strain holding, self-boring pressuremeter test. *Computers and Geotechnics*, *30*(2), 121–140.

Kaplarević-Mališić, A., Andrijević, B., Bojović, F., Nikolić, S., Krstić, L., Stojanović, B., & Ivanović, M. (2023). Identifying optimal architectures of physics-informed neural networks by evolutionary strategy. *Applied Soft Computing*, *146*, 110646.

Karniadakis, G. E., Kevrekidis, I. G., Lu, L., Perdikaris, P., Wang, S., & Yang, L. (2021). Physics-informed machine learning. *Nature Reviews Physics*, *3*(6), 422–440.

Kashefi, A., & Mukerji, T. (2023). Prediction of fluid flow in porous media by sparse observations and physics-informed pointnet. *Neural Networks*, *167*, 80–91.

Kingma, D. P., & Ba, J. (2014). Adam: A method for stochastic optimization, arXiv preprint:1412.6980.

Li, L., Fu, Y., Fung, J. C., Qu, H., & Lau, A. K. (2021). Development of a back-propagation neural network and adaptive grey wolf optimizer algorithm for thermal comfort and energy consumption prediction and optimization. *Energy and Buildings*, *253*, 111439.

Li, L., Li, J., Sun, D. A., & Gong, W. (2017). Analysis of time-dependent bearing capacity of a driven pile in clayey soils by total stress method, *International Journal of Geomechanics*, *17*(7), 04016156.

Li, L., Zhang, Y., Fung, J. C., Qu, H., & Lau, A. K. (2022). A coupled computational fluid dynamics and back-propagation neural network-based particle swarm optimizer algorithm for predicting and optimizing indoor air quality. *Building and Environment*, *207*, 108533.

Liu, M., Vashisth, D., Grana, D., & Mukerji, T. (2023). Joint identification of geophysical data for geologic carbon sequestration monitoring: a differentiable physics-informed neural network model. *Journal of Geophysical Research: Solid Earth*, *128*(3), e2022JB025372.

Lu, L., Meng, X., Mao, Z., & Karniadakis, G. E. (2021). Deepxde: A deep learning library for solving differential equations. *SIAM Review*, *63*(1), 208–228.

Lu, M., Jing, H., Wang, B., & Xie, K. (2017). Consolidation of composite ground improved by granular columns with medium and high replacement ratio. *Soils and Foundations*, *57*(6), 1088–1095.

Luo, H., & Paal, S. G. (2023). A data-free, support vector machine-based physics-driven estimator for dynamic response computation. *Computer-Aided Civil and Infrastructure Engineering*, *38*(1), 26–48.

My Ha, D., Pao-Hsiung, C., Jian Cheng, W., & Chin Chun, O. (2022). Physics-informed neural network with numerical differentiation for modelling complex fluid dynamic problems. In *International conference on offshore mechanics and arctic engineering* (Vol. *85925*, pp. V007T008A001). American Society of Mechanical Engineers.

Nabian, M. A., Gladstone, R. J., & Meidani, H. (2021). Efficient training of physics-informed neural networks via importance sampling. *Computer-Aided Civil and Infrastructure Engineering*, *36*(8), 962–977.

Naderpoor Shad , P., & Taghikhany, T. (2022). Seismic adaptive control of building structures with simultaneous sensor and damper faults based on dynamic neural network. *Computer-Aided Civil and Infrastructure Engineering*, *37*(11), 1402–1416.

Ngo, Q. H., Nguyen, B. L., Vu, T. V., Zhang, J., & Ngo, T. (2024). Physics-informed graphical neural network for power system state estimation. *Applied Energy*, *358*, 122602.

Olivier, A., Mohammadi, S., Smyth, A., & Adams, M. (2023). Bayesian neural networks with physics-aware regularization for probabilistic travel time modeling. *Computer-Aided Civil and Infrastructure Engineering*, *38*(18), 2614–2631.

Paszke, A., Gross, S., Chintala, S., Chanan, G., Yang, E., DeVito, Z., Lin, Z., Desmaison, A., Antiga, L., & Lerer, A. (2017). Automatic differentiation in Pytorch. In *31st conference on neural information processing systems (NIPS 2017)* (pp. 1–4).Long Beach, CA, USA.

Pereira, D. R., Piteri, M. A., Souza, A. N., Papa, J. P., & Adeli, H. (2020). FEMa: A finite element machine for fast learning. *Neural Computing and Applications*, *32*, 6393–6404.

Rafiei, M. H., & Adeli, H. (2017). A new neural dynamic classification algorithm. *IEEE Transactions on Neural Networks and Learning Systems*, *28*(12), 3074–3083.

Rafiei, M. H., Gauthier, L. V., Adeli, H., & Takabi, D. (2022). Self-supervised learning for electroencephalography. *IEEE Transactions on Neural Networks and Learning Systems*, *35*(2), 1457–1471.

Rall, L. B. (1981). *Automatic differentiation: Techniques and applications*, Springer.

Sajedi, S. M., & Liang, X. (2022). Deep generative Bayesian optimization for sensor placement in structural health monitoring. *Computer-Aided Civil and Infrastructure Engineering*, *37*(9), 1109–1127.

Gutierrez Soto, M., & Adeli, H. (2013). Placement of control devices for passive, semi-active, and active vibration control of structures. *Scientia Iranica*, *20*(6), 1567–1578.

Shukla, S., Sivakugan, N., & Das, B. (2009). Methods for determination of the coefficient of consolidation and field observations of time rate of settlement—An overview. *International Journal of Geotechnical Engineering*, *3*(1), 89–108.

Yuan, B., Heitor, A., Wang, H., & Chen, X. (2024). Physics-informed deep learning to solve three-dimensional Terzaghi consolidation equation: Forward and inverse problems, arXiv preprint:2401.05439.

Zhang, P., Yin, Z. Y., & Sheil, B. (2023). A physics-informed data-driven approach for consolidation analysis. *Géotechnique*, *74*(7), 1–12.

Zobeiry, N., & Humfeld, K. D. (2021). A physics-informed machine learning approach for solving heat transfer equation in advanced manufacturing and engineering applications. *Engineering Applications of Artificial Intelligence*, *101*, 104232.

How to cite this article: Gong, W., Zuo, L., Li, L., & Wang, H. (2024). Prediction of stratified ground consolidation via a physics-informed neural network utilizing short-term excess pore water pressure monitoring data. *Computer-Aided Civil and Infrastructure Engineering*, 1–19. https://doi.org/10.1111/mice.13326